buildings

MDPI

*Article*

# Experimental Investigation on the Axial Loading Performance of Grooving-Damaged Square Hollow Concrete-Filled Steel Tube Columns

**Jing Liu [1], Zimao Pan [1], Zhicheng Pan [2,3], Shaohua He [4,*] and Wenzhuo Yu [1]**

[1] Hunan Engineering Research Center of Development and Application of Ceramsite Concrete Technology, Hunan City University, Yiyang 413000, China; liujing@hncu.edu.cn (J.L.); vip_kang1314@163.com (Z.P.); thewaves710@gmail.com (W.Y.)
[2] Sinohydro Engineering Bureau 8 Co., Ltd., Changsha 410004, China; panzhichengcsu@163.com
[3] Power China Chizhou Changzhi Prefabricated Construction Co., Ltd., Chizhou 247100, China
[4] School of Civil and Transportation Engineering, Guangdong University of Technology, Guangzhou 510000, China
* Correspondence: hesh@gdut.edu.cn

**Abstract:** Under the influence of material defects, structural grooving, environmental corrosion, and other factors in engineering, concrete-filled steel tubes incur local defects on their external surfaces that affect their structural integrity and service life. This work conducts axial compression tests on 10 grooving-damaged square hollow concrete-filled steel tube (SHCFST) columns to investigate the effect of grooving damage on their axial compressive ultimate bearing capacity and the effect of steel tubes on concrete confinement. It explores the effects of three parameters, namely, the length of grooves, presence of slots in internal and external steel tubes, and orientation of grooves, on structural static performance. This study analyzes the loading, failure mechanisms, and axial compressive ultimate bearing capacity of grooving-damaged SHCFST columns. Results indicate that grooving weakens the steel tube's confinement effect on the concrete core, reducing the axial compressive ultimate bearing capacity of specimens. On the basis of this experimental research, a method for calculating the axial compressive ultimate bearing capacity and axial compressive stiffness of grooving-damaged SHCFST columns is proposed. The calculation results closely align with experimental outcomes, providing valuable insights for related scientific research and engineering applications.

**Keywords:** grooving damage; square hollow concrete-filled steel tube column; axial compressive ultimate bearing capacity

check for updates

**Citation:** Liu, J.; Pan, Z.; Pan, Z.; He, S.; Yu, W. Experimental Investigation on the Axial Loading Performance of Grooving-Damaged Square Hollow Concrete-Filled Steel Tube Columns. *Buildings* **2024**, *14*, 87. https://doi.org/10.3390/buildings14010087

Academic Editor: Rita Bento

Received: 25 November 2023
Revised: 20 December 2023
Accepted: 27 December 2023
Published: 28 December 2023

**Copyright:** © 2023 by the authors. Licensee MDPI, Basel, Switzerland. This article is an open access article distributed under the terms and conditions of the Creative Commons Attribution (CC BY) license (https://creativecommons.org/licenses/by/4.0/).

## 1. Introduction

Concrete-filled steel tube (CFST) columns, which consist of inner and outer steel tubes and concrete filler, are widely used in construction and bridge engineering because of their simple node construction, convenient connection, and good bending resistance. Solid CFST bridge piers often experience excessive axial load-bearing capacity as engineering structures increase in height and span increased distances. Square hollow concrete-filled steel tube (SHCFST) columns and other profiles have been introduced into engineering projects to conserve materials, reduce costs, and meet bending strength requirements [1–4].

In engineering, grooving and reinforcement bar insertion into steel tubes are necessary due to the needs of some applications, such as the connection of CFST beam-to-column joints. This process weakens the steel tube's confinement effect on the concrete core at the joint and reduces cross-sectional stiffness, adversely affecting the mechanical performance of the CFST column at the joint [1–3]. He et al. [5] studied the influence of local geometric defects on the mechanical performance of CFST columns. They found that in CFST columns,

the above damage weakens mechanical properties, destroys structural integrity, and affects service life. Research has been conducted on this topic domestically and internationally.

Research on CFST columns with grooving damage includes the work of Zhu et al. [6], who performed axial compression tests on grooving-damaged circular CFST short columns fabricated by using 12 different circumferential and longitudinal grooving methods. They analyzed the effects of various grooving methods on steel tube-confined concrete. Yu et al. [7,8] conducted experimental studies on the axial compressive performance of grooving-damaged circular CFST short columns. They investigated changes in the mechanical properties, such as stiffness, load-bearing capacity, and ductility, of specimens after grooving. Chang et al. [9] performed axial compression tests on 15 grooving-damaged circular CFST short columns. They analyzed the effect of groove length and direction, concrete strength, and steel content and proposed a formula for calculating the axial compressive bearing capacity of grooving-damaged circular CFST short columns. Liu et al. [10] conducted experimental studies on 14 hexagonal CFST short columns with different groove directions, positions, and sizes. They analyzed the strain development, failure mechanisms, and axial compressive ultimate bearing capacity of grooving-damaged hexagonal CFST short columns and established a method for calculating the ultimate strength of components. Guo et al. [11] performed experimental studies on 15 groups of square CFST columns with grooves, including central transverse, longitudinal, diagonal, and edge transverse and longitudinal grooves. They explored the effects of groove length, thickness, and direction on the axial compressive bearing capacity of square CFST columns and proposed a formula for calculating the axial compressive bearing capacity of grooving-damaged square CFST columns. Han et al. [12] investigated the mechanical performance of square CFST column components after corrosion and conducted a comparative analysis of the load-bearing capacity of square CFST column components by using different standards. Alzand et al. [13] revealed the flexural performance of square CFST beams stiffened with V-shaped grooves, and the bending moment capacity and the flexural stiffness results obtained from the experimental and numerical investigations were validated with predicted values from different existing standards. Wei et al. [14] investigated the behavior of rectangular concrete-filled fiber-reinforced polymer (FRP) and steel composite tube (CFCT) columns with stress-release grooves under axial compression and found stress-release grooves only play a positive role in specimens with relatively large values of the corner radii.

Studies on SHCFST columns include the research of Zhao et al. [15], who established theoretical models for the ultimate strength of SHCFST short columns and beams by conducting a series of axial compression and bending tests on SHCFST short columns. Ayough et al. [16] performed nonlinear analyses on double-layer CFST columns under axial compression. They suggested that increasing the wall thickness of the outer steel tube can reduce the sensitivity of the steel tube to local buckling, thereby improving the overall performance of columns. Muhammad Rizwan et al. [17] developed a calculation modeling method using fiber discretization technology. Their method considerably saved model development and computation time compared with finite element methods. They proposed an expression for designing rectangular hollow CFST columns and concluded that the yield stress of the steel had no remarkable effect on the ductility of columns. Ding et al. [18] create a three-dimensional solid model that considered the effects of various parameters on the ultimate bearing capacity and pressure stresses of concrete. They proposed practical calculation formulas for the load-bearing capacity of SHCFST short columns. Guo et al. [19] subjected 10 square CFST short columns with double inner steel tubes to axial compression tests. They systematically studied the influence of concrete strength, eccentricity, and section slenderness on the strength, deformation, and ductility of the specimens, presenting a simplified calculation formula for the ultimate strength of hollow CFST short columns.

As can be observed from the abovementioned works, research on the axial compression of grooving-damaged SHCFST columns is limited. By building on existing research, our research group (1) conducted axial compression tests on 10 grooving-damaged SHCFST columns; (2) analyzed the effect of three different grooving defect factors, including the

length of grooves, presence of slots in internal and external steel tubes (number of grooves), and direction of grooves, on the mechanical performance of SHCFST columns; and (3) recommended a formula for the bearing capacity of grooving-damaged SHCFST columns by utilizing the bearing capacity formula for SHCFST columns proposed by Ding [18].

## 2. Experimental Study

### *2.1. Test Design*

Ten grooving-damaged SHCFST columns with three varying parameters, namely, the length of grooves, presence of slots in internal and external steel tubes (number of grooves), and orientation of grooves, were designed for the experiments. Table 1 shows the specimen size and material characteristics of a CFST column. All specimens had the same cross-sectional dimensions. Prior to testing, the material properties of the steel as well as the mechanical properties of cubic concrete specimens were determined in accordance with standard testing methods. The specimens are depicted in Figure 1, wherein $l$ is the length of the steel tube groove, $b$ is the width of the steel tube groove, $D$ is the outer square side length, $t$ is the steel material thickness, $H$ is the specimen height, $f_s$ denotes the yield strength of the steel material, $f_{cu}$ indicates the compressive strength of cubic concrete specimens, and $p$ is the specimen perimeter.

**Table 1.** Specimen size and material characteristics of CFST column.

| | No. | Orientation | Location | $L \times b$ (mm) | $D \times t \times H$ (mm) | $f_s$ (MPa) | $f_{cu}$ (MPa) | $N_t$ (kN) | $N_c$ (kN) |
|---|---|---|---|---|---|---|---|---|---|
| 1 | SHCFST-1 | Vertical | Inside and outside | 120 × 16 | 200 × 2.8 × 600 | 359 | 29.6 | 1500 | 1458.8 |
| 2 | SHCFST-2 | Vertical | Inside and outside | 80 × 16 | 200 × 2.8 × 600 | 359 | 29.6 | 1570 | 1591.8 |
| 3 | SHCFST-3 | Vertical | Inside and outside | 40 × 16 | 200 × 2.8 × 600 | 359 | 29.6 | 1590 | 1724.8 |
| 4 | SHCFST-4 | Vertical | Outside | 120 × 16 | 200 × 2.8 × 600 | 359 | 29.6 | 1600 | 1665.0 |
| 5 | SHCFST-5 | Vertical | Outside | 80 × 16 | 200 × 2.8 × 600 | 359 | 29.6 | 1723 | 1731.5 |
| 6 | SHCFST-6 | Vertical | Outside | 40 × 16 | 200 × 2.8 × 600 | 359 | 29.6 | 1755 | 1798.0 |
| 7 | SHCFST-7 | Horizontal | Inside and outside | 80 × 16 | 200 × 2.8 × 600 | 359 | 29.6 | 1774 | 1711.5 |
| 8 | SHCFST-8 | Horizontal | Inside and outside | 40 × 16 | 200 × 2.8 × 600 | 359 | 29.6 | 1803 | 1778.0 |
| 9 | SHCFST-9 | Horizontal | Outside | 80 × 16 | 200 × 2.8 × 600 | 359 | 29.6 | 1795 | 1791.3 |
| 10 | SHCFST-10 | Horizontal | Outside | 40 × 16 | 200 × 2.8 × 600 | 359 | 29.6 | 1824 | 1824.6 |

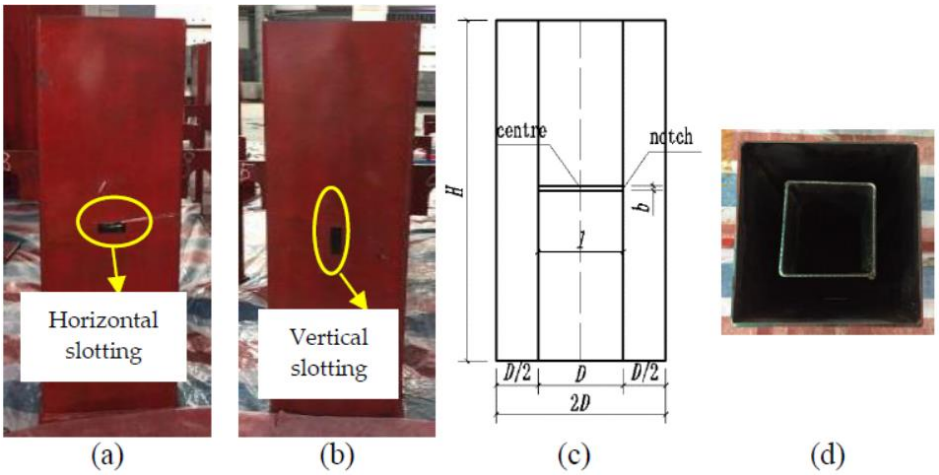



**Figure 1.** Solid and dimensional diagram of a CFST column slotted specimen. (**a**) Horizontal slotted specimen; (**b**) vertically slotted specimen; (**c**) specimen size diagram; (**d**) top view of steel tube.

Thin-walled steel tubes were formed by bending and welding thin plates. By contrast, the surfaces of square steel tubes were welded together from two L-shaped steel plates after crimping, and the inner and outer square steel tubes had two welds, as shown in Figure 1d. During production, it was ensured that the cross sections at both ends of the steel tube

were smooth and without distortion. A 3 mm thick steel plate was welded to the bottom of the formed steel tube. The locations and sizes for groove preparation were positioned and marked on the steel tube, and a cutting machine was carefully used to create grooves on the steel tube corresponding to specifications. Tape was used to seal the grooved area when pouring concrete. The steel tube was then erected. Concrete was poured from the top and compacted with a vibrating rod until it was densely packed. The concrete at the ends was smoothed. The specimens were naturally cured.

### *2.2. Loading Scheme*

Tests were conducted by using a 5000 kN hydrostatic machine for loading. The experimental setup for the SHCFST columns and field test are illustrated in Figure 2. Resistive strain gauges were installed along the midsection of the specimens, as shown in Figure 2a, to measure their vertical and horizontal deformations.




**Figure 2.** CFST columns test device and field test diagram. (**a**) Test apparatus; (**b**) field test.

A displacement-controlled loading procedure was employed. During the elastic and plastic phase, each load level was approximately 1/15th of the ultimate load, and each load level was sustained for approximately half a minute. Loading was maintained at a slow, continuous pace, and corresponding data were synchronously collected. As the specimens approached their ultimate load-bearing capacity, they were slowly and continuously loaded until failure. Each test on the specimens lasted for approximately 10 min. In accordance with the characteristics of the specimen, the test was interrupted when the axial displacement reached 0.025 H.

### *2.3. Loading Phenomenon*

SHCFST columns affixed with strain gauges were placed at the premarked center of the loading platform. A preliminary preload was applied to the SHCFST columns by using a hydrostatic machine to eliminate any gaps between the hydrostatic machine and upper surface of the SHCFST columns. Subsequently, the displacement dial indicator was zeroed in preparation for the start of the test. The SHCFST-1 specimen, which had vertical internal and external grooves 120 mm in length, were used to illustrate loading. Representative stages during loading are depicted in Figure 3.

When the load reached 200 kN, the axial displacement of the specimen was 0.20 mm, indicating the early stage of the elastic phase. At this point, no remarkable buckling or other deformations were observed on the surface of the specimen. Under a load of 1000 kN, the axial displacement of the specimen was 1.11 mm, signifying the initial stage of the elastic–plastic phase. Slight buckling was observed on the upper external steel tube of the specimen. At an axial displacement of 3.01 mm and a loading of 1500 kN, the specimen was on the verge of failure. Audible sounds of material compression and fracture could be heard at the test site. The degree of buckling on the outer steel tube of the upper section of

the specimen continued to increase. At an axial displacement of 7.15 mm, the specimen entered the failure stage. The load reading on the hydrostatic machine had dropped from its peak of 1500 kN to 1098 kN by this point. The buckling of the upper external steel tube had drastically increased and was spreading downward. As the load decreased to 711 kN and the axial displacement of the specimen reached 15.84 mm, buckling was observed to have extended from the middle to the top four corners of the specimen. Loading was stopped to prevent the specimen from bursting.

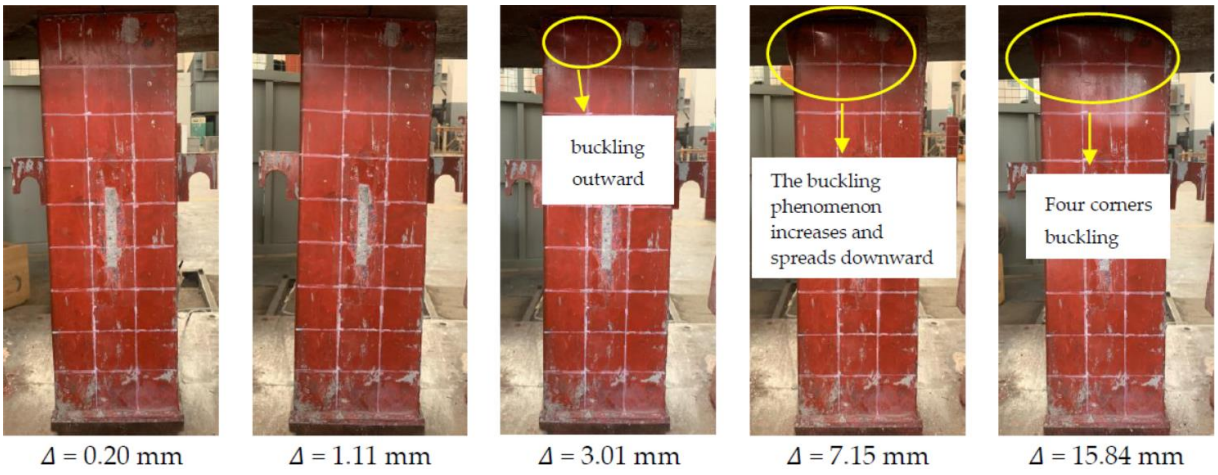



**Figure 3.** Several representative stages during the loading process.

As depicted in Figure 4, which illustrates the typical failure modes of the specimens, all specimens experienced buckling phenomenon at their top or bottom during the test.

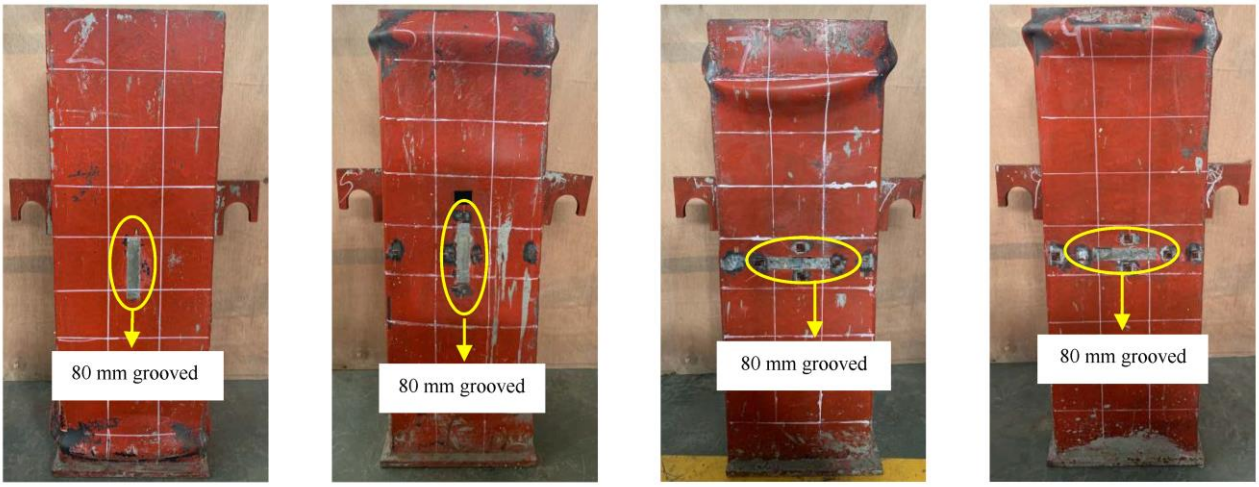



**Figure 4.** Failure patterns of typical specimens.

After the completion of the experiments, the steel tube of the specimens was cut and stripped to reveal the condition of the concrete core, as shown in Figure 5. The following observations were obtained: (1) specimens with vertical grooves lacked apparent signs of concrete damage in their grooved section. However, they exhibited noticeable concrete damage near their grooved section and at their upper and lower parts, as depicted in Figure 5a,b. (2) Specimens with horizontal grooves showed minor concrete damage in their grooved section but considerable concrete damage in their upper part, as shown in Figure 5c,d. (3) The concrete core failure of the specimens with inner and outer steel tube grooves was more obvious than that of the specimens with only outer steel tube grooves.

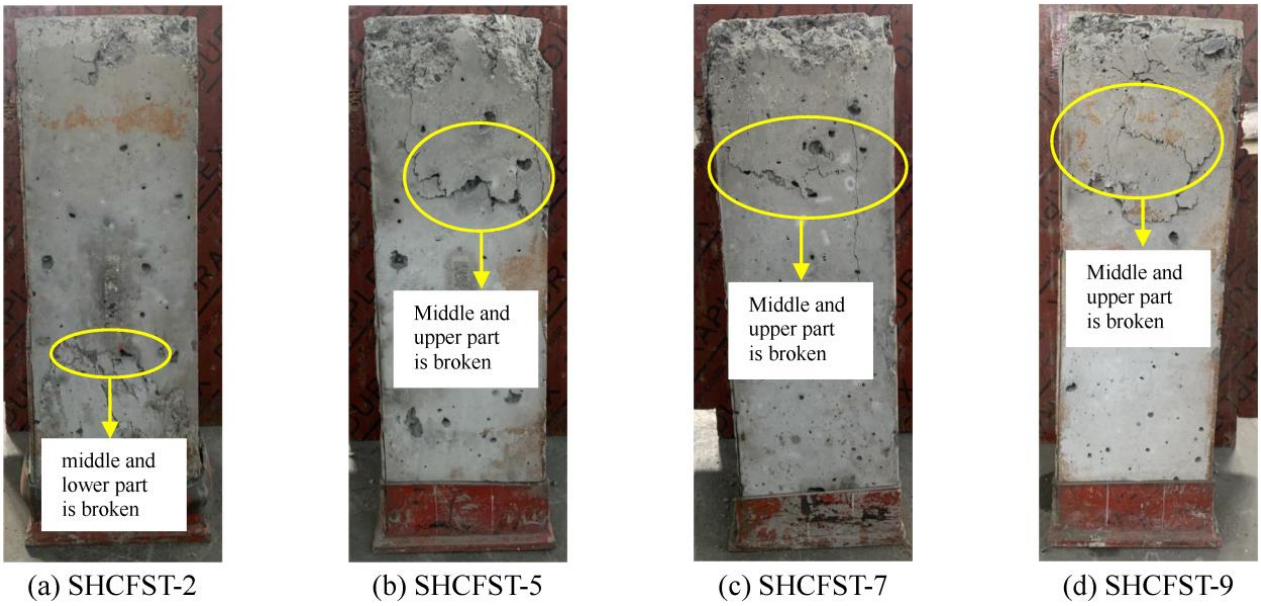



**Figure 5.** Failure patterns of core concrete of typical specimens.

### *2.4. Analysis of Test Results*

Figure 6 illustrates the load–displacement curves of the specimens. The static test on the steel tube concrete columns can be divided into three stages: elastic, elastic–plastic, and failure stages. (1) Elastic stage: During the initial loading stage (approximately 60% of the ultimate load), the axial deformation of the specimens exhibited nearly linear growth as the load increased. The appearance of the specimens remained unchanged. (2) Elastic–plastic stage: After surpassing the yield load, the load–deflection curve exhibited nonlinear growth. The linear growth in axial displacement decelerated as the load increased, showing a gradual upward trend. The appearance of the specimens still did not show any remarkable change. (3) Failure stage: After reaching the ultimate load, the buckling of the specimen was aggravated with the increase in axial deformation.

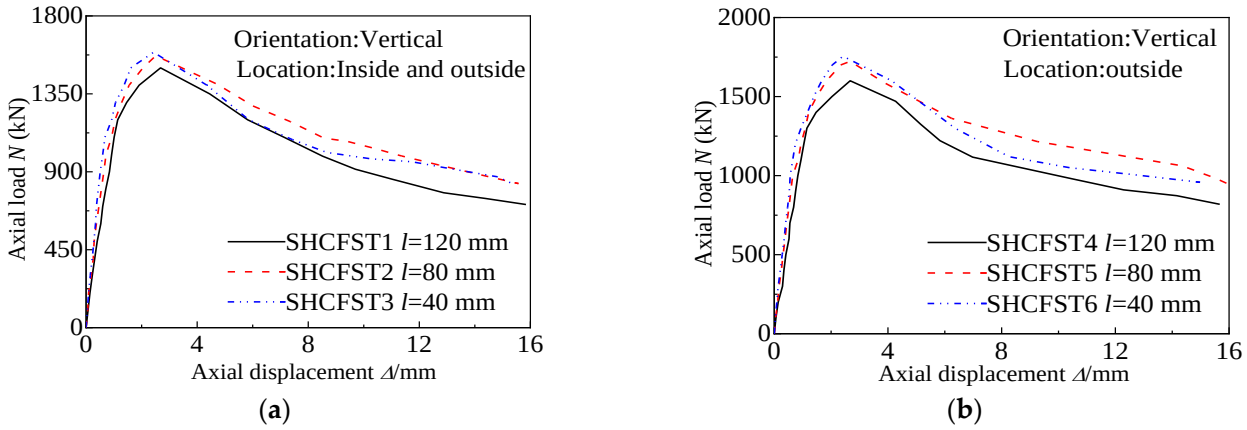



**Figure 6.** *Cont.*

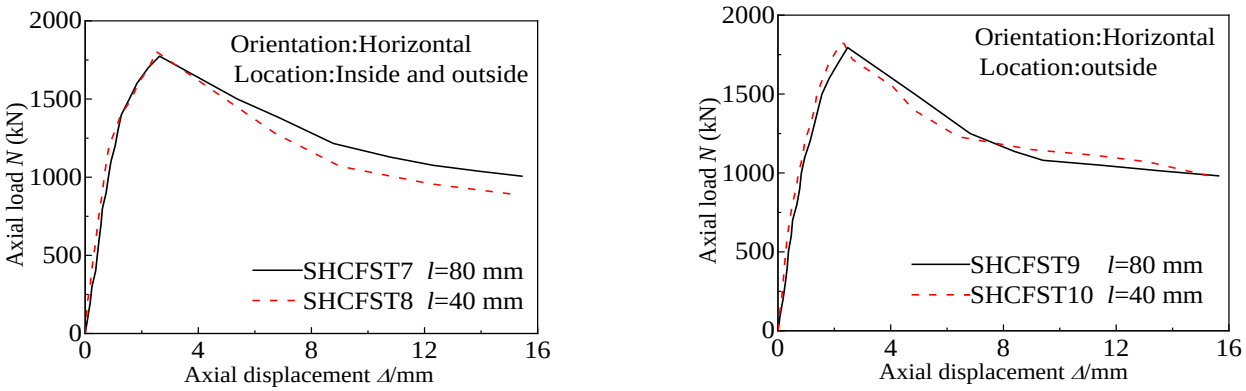



**Figure 6.** Load–displacement curve of specimens. (**a**) SHCFST1~SHCFST3; (**b**) SHCFST4~SHCFST6; (**c**) SHCFST7~SHCFST8; (**d**) SHCFST9~SHCFST10.

## 3. Effects of Three Parameters on the Axial Compression Performance of SHCFST Columns

### *3.1. Influence of Notch Length*

Figure 7 depicts the influence of notch length on the load-bearing performance of SHCFST columns. The groove lengths tested were 40, 80, and 120 mm. As the groove length increases, the steel tube's constraining effect weakens, leading to the low ultimate load-bearing capacity of the specimens.

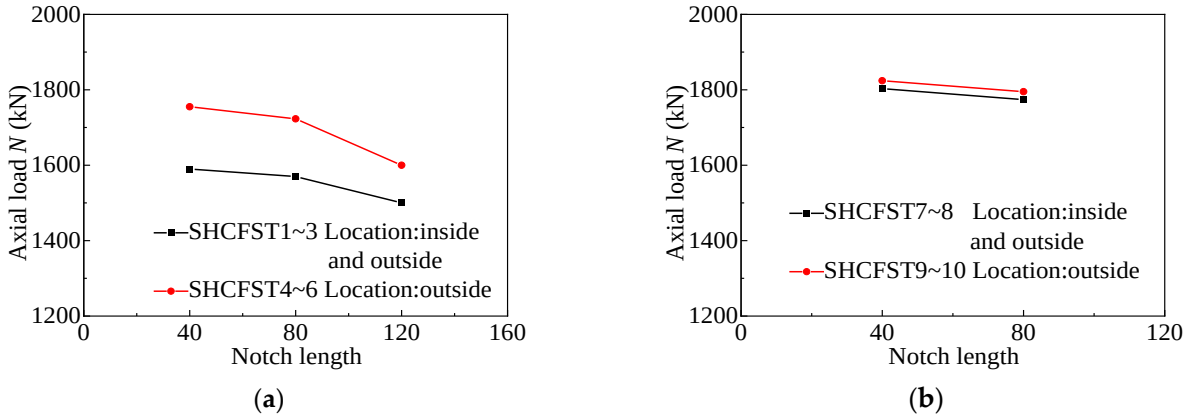



**Figure 7.** Influence of notch length on the ultimate strength of specimens. (**a**) SHCFST1~SHCFST6; (**b**) SHCFST7~SHCFST10.

For specimens with vertical grooves, the load-bearing capacity of the specimen with inner and outer steel tube groove lengths of 40 mm is 1.3% and 6.0% greater than that of the specimens with groove lengths of 80 and 120 mm, respectively. The load-bearing capacity of the specimen with an external groove length of 40 mm is 1.9% and 9.7% greater than that of the specimens with groove lengths of 80 and 120 mm, respectively.

For specimens with horizontal grooves, the load-bearing capacity of the specimen with inner and outer steel tube groove lengths of 40 mm is 1.6% greater than that of the specimen with an 80 mm groove length, and the specimen with an external groove length of 40 mm has a load-bearing capacity that is 4.0% greater than that of the specimen with an 80 mm groove length.

### *3.2. Influence of Notch Location*

Figure 8 illustrates the effect of the presence of internal and external grooves on the load-bearing performance of SHCFST columns with grooves in their internal central and external central parts. When the inner and outer steel tubes are slotted, the ultimate bearing

capacity of the SHCFST column is smaller than that when only the outer steel tube is slotted.

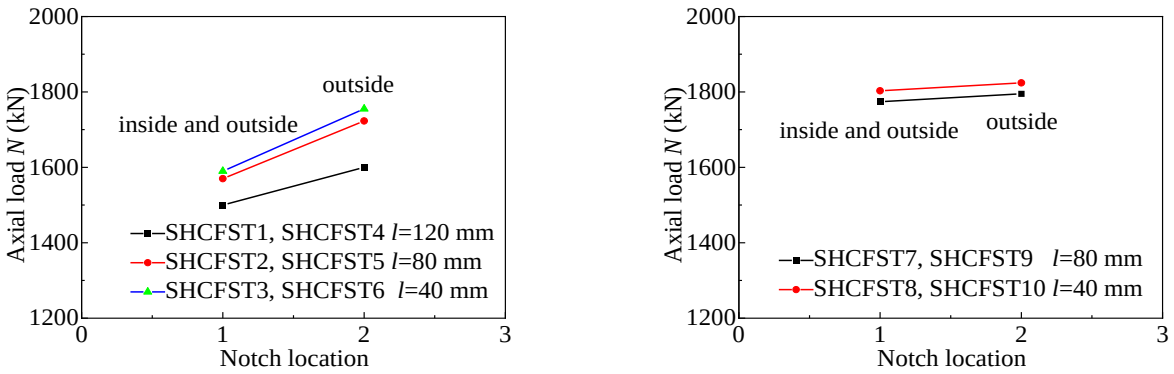



**Figure 8.** Influence of slot position on the ultimate load force of the specimen. (**a**) SHCFST1~SHCFST6; (**b**) SHCFST7~SHCFST10.

For specimens with vertical grooves, the load-bearing capacity of specimens with external grooves is 8.9% greater than that of specimens with inner and outer steel grooves. For specimens with horizontal grooves, the load-bearing capacity of specimens with external grooves is approximately 1.2% greater than that of specimens with inner and outer steel grooves.

### *3.3. Influence of Notch Direction*

Figure 9 illustrates the effect of groove direction on the load-bearing performance of SHCFST columns, with groove directions being vertical and horizontal. When internal and external grooves are present, the load-bearing capacity of specimens with horizontal grooves is 13.0% greater than that of specimens with vertical grooves. When only external grooves are present, the load-bearing capacity of specimens with horizontal grooves is 11.2% greater than that of specimens with vertical grooves.

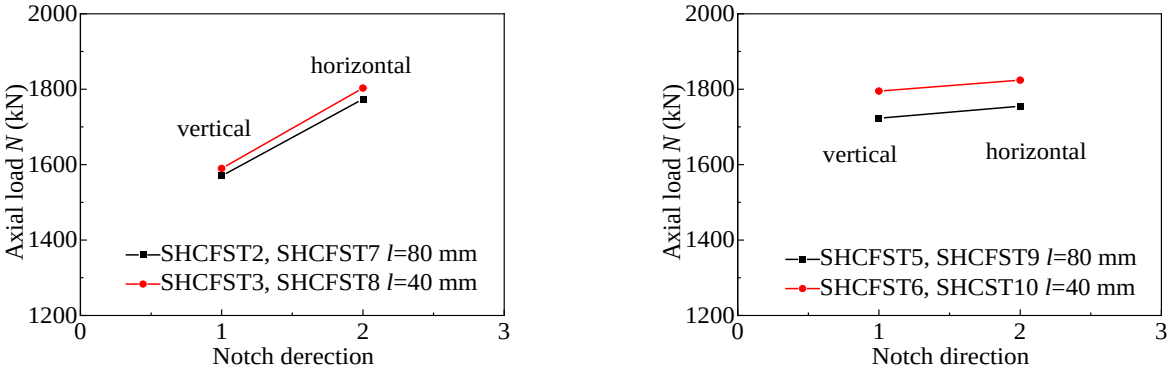



**Figure 9.** Influence of groove direction on the ultimate load force of the specimen. (**a**) Specimens with grooves both inside and outside steel tubes; (**b**) specimens with grooves outside steel tubes.

## 4. Calculation of the Ultimate Bearing Capacity and Axial Compression Stiffness of Notched SHCFST Columns

### *4.1. Bearing Strength*

The following formula proposed in the literature [18] is adopted for SHCFST column specimens without grooves:

$$N_c = f_c A_c + K f_{so} A_{so} + f_{si} A_{si}, \quad (1)$$

where $N_c$ is the calculated capacity of columns; $A_c$ is the section area of concrete; $f_c$ is the compressive strength of concrete, $f_c = 0.4f_{cu}^{7/6}$; and $K$ is the constraint coefficient of the concrete-filled steel tube. Ding et al. [18] reported that for SHCFST column specimens with hollow ratios between 0 and 0.77, $K = 1.2 + 0.15X_o - 0.3\sqrt{X_o}$, where $X_o$ is the hollow ratio. The steel test specimen has square internal and external cross sections; 100 and 200 mm inner and outer edges, respectively; and calculated $K$ = 1.08. $f_{so}$ and $A_{so}$ are the yield strength and area of the outer steel tube, respectively, and $f_{si}$ and $A_{si}$ are the yield strength and area of the inner steel tube, respectively.

The discussion of the above experimental results reveals that the length, number, and direction of grooves have a certain effect on the ultimate load-bearing capacity of composite columns. Therefore, the following equation for calculating the ultimate load-bearing capacity of grooved SHCFST columns is proposed:

$$N_c = f_c A_c + K_1(Kf_{so}A_{so} + f_{si}A_{si}) \tag{2}$$

In the formula, the mathematical expression of $K_1$ is

$$K_1 = 1.0 - (0.8\beta_1 + 1.6\beta_2) \tag{3}$$

Here, $\beta_1$ and $\beta_2$ are the parameters related to groove length and width, number, and direction, whereas $S$ represents the perimeter of the steel material's cross section.

The following definitions are provided for specimens with inner and outer grooves:

$$\beta_1 = \begin{cases} b/H & \text{Transverse slotting} \\ b/S & \text{Vertical slotting} \end{cases}, \tag{4}$$

$$\beta_2 = \begin{cases} l/S & \text{Transverse slotting} \\ l/H & \text{Vertical slotting} \end{cases}. \tag{5}$$

The following definitions are provided for specimens with outer grooves:

$$\beta_1 = \begin{cases} 2b/H & \text{Transverse slotting} \\ 2b/S & \text{Vertical slotting} \end{cases}, \tag{6}$$

$$\beta_2 = \begin{cases} 2l/S & \text{Transverse slotting} \\ 2l/H & \text{Vertical slotting} \end{cases}. \tag{7}$$

The average $N_c/N_t$ ratio is 0.992, and the dispersion coefficient is 0.034. $N_t$ is the tested capacity of the columns. Figure 10 shows that the results calculated by using the formula are in good agreement with the test results.

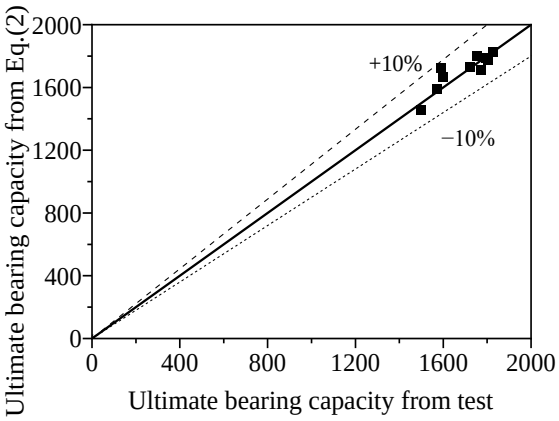



**Figure 10.** Comparison of the bearing capacity obtained through tests and Equation (2).

### *4.2. Confinement Effect*

In summary, the grooving damage of steel tube weakens the confinement effect on the concrete core, making the mechanical properties of the damaged CFST column worse than those of undamaged CFST column. Therefore, the evaluation of the confinement effect is a crucial issue. The column strength of a steel tube concrete section is the sum of contributions from the steel tube, concrete, and interaction between the steel tube and concrete. Therefore, it can be expressed as:

$$N_c = A_s f_s + A_c f_c + F_{s.} \tag{8}$$

$F_s$ is the contribution of the interaction between the steel tube and concrete, $F_s = N_c - A_s f_s - A_c f_c$.

For grooved specimens, only part of the steel tube can withstand the axial load due to the existence of notches. As can be seen from Equation (8), the column strength of grooved SHCFST columns is

$$N_c = A_{se} f_s + A_c f_c + F_s. \tag{9}$$

For specimens with internal and external vertical grooves, the effective section area $A_{se}$ of the steel tube is defined as

$$A_{se} = (1 - 2l/H) \times S. \tag{10}$$

For specimens with external vertical grooves, the effective section area $A_{se}$ of the steel tube is defined as

$$A_{se} = (1 - l/H) \times S. \tag{11}$$

For specimens with internal and external transverse grooves, the effective section area $A_{se}$ of the steel tube is defined as

$$A_{se} = (1 - 2l/p) \times S. \tag{12}$$

For specimens with external transverse grooves, the effective section area $A_{se}$ of the steel tube is defined as

$$A_{se} = (1 - l/p) \times S. \tag{13}$$

Hence, the confinement factor defined in Equation (14) was applied to estimate the confinement effect of a grooved steel tube on the concrete core:

$$\lambda = F_s/N_c. \tag{14}$$

The confinement coefficients of all tested notched specimens are shown in Table 2. The confinement factor increases as the groove length of the steel tube increases.

**Table 2.** List of constraint coefficients of specimens.

| No. | $A_{se}$ (mm$^2$) | $A_{se}f_s + A_cf_c$ (kN) | $N_c$ (kN) | $F_s$ (kN) | $\lambda$ |
|---|---|---|---|---|---|
| SHCFST-1 | 2016.0 | 1348.5 | 1458.8 | 110.3 | 0.076 |
| SHCFST-2 | 2464.0 | 1509.3 | 1591.8 | 82.5 | 0.052 |
| SHCFST-3 | 2912.0 | 1670.1 | 1724.8 | 54.7 | 0.032 |
| SHCFST-4 | 2688.0 | 1589.7 | 1665.0 | 75.3 | 0.045 |
| SHCFST-5 | 2912.0 | 1670.1 | 1731.5 | 61.4 | 0.035 |
| SHCFST-6 | 3136.0 | 1750.5 | 1798.0 | 47.5 | 0.026 |
| SHCFST-7 | 2464.0 | 1509.3 | 1711.5 | 202.2 | 0.118 |
| SHCFST-8 | 2912.0 | 1670.1 | 1778.0 | 107.9 | 0.061 |
| SHCFST-9 | 3136.0 | 1750.5 | 1791.3 | 40.8 | 0.023 |
| SHCFST-10 | 3248.0 | 1790.8 | 1824.6 | 33.8 | 0.019 |

For specimens with vertical grooves, the confinement factor of the specimen with the internal and external steel tube groove length of 120 mm is 139% and 45.9% greater than that of the specimens with 40 and 80 mm groove lengths, respectively. The load-bearing capacity of the specimen with an external groove length of 120 mm is 71.3% greater than that of the specimen with an 80 mm groove length and 27.6% greater than that of the specimen with an 80 mm groove length.

For specimens with horizontal grooves, the load-bearing capacity of the specimen with internal and external steel tube groove lengths of 80 mm is 94.7% greater than that of the specimen with a 40 mm groove length, and the specimen with an external groove length of 80 mm has a load-bearing capacity that is 22.6% greater than that with a 40 mm groove length.

That is, the damage caused by the grooving of the steel tube has a considerable effect on structural bearing capacity and exhibits a nonlinear relationship. In engineering applications, grooving should receive careful consideration.

### *4.3. Axial Compression Stiffness*

In this study, the ultimate load corresponding to 50% of the specimen's limit load is taken and associated with the secant stiffness at the axial compression stiffness of the specimen. $(EA)_c$ is defined as

$$(EA)_c = E_s A_{se} + E_c A_c. \quad (15)$$

Figure 10 shows the axial compression stiffness of the specimens. $(EA)_t$ is the measured axial compressive stiffness of the specimens. The average $(EA)_t/(EA)_c$ is 0.952, and the dispersion coefficient is 0.132. The results obtained with Equation (15) are in good agreement with the experimental results. Table 3 shows the List of axial compression stiffness of specimens.

**Table 3.** List of axial compression stiffness of specimens.

| No. | $E_s$ (Pa) | $E_c$ (Pa) | $A_{se}$ (mm$^2$) | $A_c$ (mm$^2$) | $(EA)_c$ (N) | $(EA)_t$ (N) | $(EA)_c/(EA)_t$ |
|---|---|---|---|---|---|---|---|
| SHCFST-1 | $2.06 \times 10^{11}$ | $3.35 \times 10^{10}$ | 2016.0 | 30,000 | $1.420 \times 10^{9}$ | $1.11 \times 10^{9}$ | 0.821 |
| SHCFST-2 | $2.06 \times 10^{11}$ | $3.35 \times 10^{10}$ | 2464.0 | 30,000 | $1.513 \times 10^{9}$ | $1.52 \times 10^{9}$ | 1.006 |
| SHCFST-3 | $2.06 \times 10^{11}$ | $3.35 \times 10^{10}$ | 2912.0 | 30,000 | $1.605 \times 10^{9}$ | $1.89 \times 10^{9}$ | 1.179 |
| SHCFST-4 | $2.06 \times 10^{11}$ | $3.35 \times 10^{10}$ | 2688.0 | 30,000 | $1.559 \times 10^{9}$ | $1.23 \times 10^{9}$ | 0.817 |
| SHCFST-5 | $2.06 \times 10^{11}$ | $3.35 \times 10^{10}$ | 2912.0 | 30,000 | $1.605 \times 10^{9}$ | $1.59 \times 10^{9}$ | 0.991 |
| SHCFST-6 | $2.06 \times 10^{11}$ | $3.35 \times 10^{10}$ | 3136.0 | 30,000 | $1.651 \times 10^{9}$ | $1.75 \times 10^{9}$ | 1.060 |
| SHCFST-7 | $2.06 \times 10^{11}$ | $3.35 \times 10^{10}$ | 2464.0 | 30,000 | $1.513 \times 10^{9}$ | $1.25 \times 10^{9}$ | 0.826 |
| SHCFST-8 | $2.06 \times 10^{11}$ | $3.35 \times 10^{10}$ | 2912.0 | 30,000 | $1.605 \times 10^{9}$ | $1.60 \times 10^{9}$ | 0.991 |
| SHCFST-9 | $2.06 \times 10^{11}$ | $3.35 \times 10^{10}$ | 3136.0 | 30,000 | $1.651 \times 10^{9}$ | $1.21 \times 10^{9}$ | 0.815 |
| SHCFST-10 | $2.06 \times 10^{11}$ | $3.35 \times 10^{10}$ | 3248.0 | 30,000 | $1.674 \times 10^{9}$ | $1.67 \times 10^{9}$ | 0.996 |

## 5. Conclusions

This work conducted axial compression tests on 10 grooving-damaged SHCFST column specimens. It investigated the influence of parameters, such as the length of grooves, presence of grooves in internal and external steel tubes (number of grooves), and direction of grooves, on the load-bearing performance of steel tube concrete columns. This study examined structural failure modes, load–displacement curves, and other performance aspects. Additionally, it proposed an equation for calculating the ultimate load-bearing capacity and axial compression stiffness of grooving-damaged SHCFST columns. Its main conclusions are as follows:

(1) The test results indicate that at the early stage of the elastic phase, no remarkable buckling or other deformations are present on the surface of the specimen. Different types of CFST columns exhibit the same failure modes. That is, all specimens experience buckling phenomenon at their top or bottom. After the completion of the experiments, the steel tube of the specimens was cut and stripped, which revealed

the core concrete had different degrees of damage. The concrete core failure of the specimens with inner and outer steel tube grooves was more obvious than that of the specimens with only outer steel tube grooves;

(2) The ultimate load-bearing capacity of grooved CFST columns is lower than that of intact CFST columns because grooved steel tubes cannot provide sufficient constraint to the concrete core within the column. Parameter analysis reveals that groove length and width, position, and direction have a certain effect on the strength of concrete columns in grooved steel tubes. It can be observed that as the groove length increases, the steel tube's constraining effect weakens, leading to the low ultimate load-bearing capacity of the specimens. When the inner and outer steel tubes are slotted, the ultimate bearing capacity of the SHCFST column is smaller than that when only the outer steel tube is slotted. The load-bearing capacity of specimens with horizontal grooves is greater than that of specimens with vertical grooves;

(3) The ultimate load-bearing capacity of undamaged SHCFST columns was predicted by using existing formulas. An empirical equation based on the formula proposed by Ding et al. [18] was established to predict the ultimate load-bearing capacity of grooved SHCFST columns. The calculated values align well with the experimental results. This work also proposes the confinement effect. Experiments indicate that grooving has a considerable influence on structural load-bearing capacity and has a nonlinear relationship;

(4) The influence of damage caused by grooving in steel tubes is considered, and a formula for calculating the axial compression stiffness of the specimens is proposed. The calculation results are in good agreement with the experimental results.

**Author Contributions:** Writing—original draft, Funding acquisition, Data curation, J.L.; Formal analysis, Investigation, Z.P. (Zimao Pan); Methodology, Validation, Z.P. (Zhicheng Pan); Supervision, Visualization Preparation, Writing—review and editing, S.H.; Resources, Data curation, W.Y.; All authors have read and agreed to the published version of the manuscript.

**Funding:** National Natural Science Foundation of China: 52008159; Hunan Education Department Foundation Funded Project: 21A0504; Natural Science Foundation of Hunan Province: 2022JJ30112; Key research and development project of Anhui Province: 2022o07020003; Anhui Province Housing and Urban Rural Construction Science and Technology Plan Project: 2023-YF-112.

**Data Availability Statement:** The data presented in this study are available on request from the corresponding author. The data are not publicly available due to privacy.

**Conflicts of Interest:** Author Zhicheng Pan was employed by the companies Sinohydro Engineering Bureau 8 Co., Ltd. and Power China Chizhou Changzhi Prefabricated Construction Co., Ltd. The remaining authors declare that the research was conducted in the absence of any commercial or financial relationships that could be construed as a potential conflict of interest.

## References

1. Zhou, X.H.; Cheng, G.Z.; Liu, J.P.; Gan, D.; Chen, Y.F. Behavior of circular tubed-RC column to RC beam connections under axial compression. *J. Constr. Steel Res.* **2017**, *130*, 96–108. [CrossRef]
2. Tian, C.Y.; Xiao, C.Z.; Chen, T.; Fu, X.Y. Experimental study on through beam connection system for concrete filled steel tube column-RC beam. *Steel Compos. Struct.* **2014**, *16*, 187–201. [CrossRef]
3. He, S.H.; Zhou, W.J.; Jiang, Z.; Zheng, C.; Mo, X.; Huang, X. Structural performance of perforated steel plate-CFST arch feet in concrete girder-steel arch composite bridges. *J. Constr. Steel Res.* **2023**, *201*, 107742. [CrossRef]
4. Zarringol, M.; Chen, Y.; Wang, Y.; Jiang, M.Y. Application of machine learning models for designing CFCFST columns. *J. Constr. Steel Res.* **2021**, *185*, 106856. [CrossRef]
5. He, S.H.; Fang, Z.; Mosallam, A.M.; Ou, Y.Y.; Zou, C. Behavior of CFSC encased shear connectors in steel-concrete joints: Push-out tests. *J. Struct. Eng.* **2020**, *146*, 04020015. [CrossRef]
6. Zhu, X.J.; Lu, J.F.; Hou, S.M. Experimental study on axial compression of notched concrete filled steel column. In Proceedings of the 7th National Conference on Structural Engineering (Vol. II), Shijiazhuang, China, 2 July 1998; pp. 218–222.
7. Yu, Z.Y.; Ding, F.X.; Cai, C.S. Experimental behavior of circular concrete-filled steel tube stub columns. *J. Constr. Steel Res.* **2007**, *63*, 165–174. [CrossRef]

8. Chen, Z.P.; Zhong, M.; Chen, Y.L. Experimental study on mechanical properties of concretefilled opening hole damaged steel tubular members. *Ind. Constr.* **2013**, *43*, 121–127. (In Chinese)
9. Chang, X.; Fu, L.; Zhao, H.B.; Zhang, Y.B. Behaviors of axially loaded circular concrete-filled steel tube (CFT) stub columns with notch in steel tubes. *Thin-Walled Struct.* **2013**, *73*, 273–280. [CrossRef]
10. Liu, J.; Li, Z.; Ding, F.X. Experimental investigation on the axially loaded performance of notched hexagonal concrete-filled steel tube (CFST) column. *Adv. Civ. Eng.* **2019**, *2019*, 2612536. [CrossRef]
11. Guo, L.H.; Huang, H.J.; Chen, J.; Romanov, K. Axial behavior of square CFST with local corrosion simulated by artificial notch. *J. Constr. Steel Res.* **2020**, *174*, 106314. [CrossRef]
12. Han, L.H.; Hou, C.; Wang, Q.L. Square concrete filled steel tubular (CFST) members under loading and chloride corrosion: Experiments. *J. Constr. Steel Res.* **2012**, *71*, 11–25. [CrossRef]
13. Alzand, A.W.; Badaruzzaman, W.H.W.; Shaikhli, M.S.; Ali, M.M. Flexural performance of square concrete-filled steel tube beams stiffened with V-shaped grooves. *J. Constr. Steel Res.* **2020**, *166*, 105930. [CrossRef]
14. Wei, Y.; Zhu, C.; Miao, K.T.; Cai, J.L.; Zheng, K.Q. Compressive behavior of rectangular concrete-filled fiber-reinforced polymer and steel composite tube columns with stress-release grooves. *Compos. Struct.* **2022**, *281*, 114983. [CrossRef]
15. Zhao, X.L.; Grzebieta, R. Strength and ductility of concrete filled double skin (SHS inner and SHS outer) tubes. *Thin-Walled Struct.* **2002**, *40*, 199–213. [CrossRef]
16. Ayough, P.; Sulong, N.H.R.; Ibrahim, Z.; Hsiao, P.C. Nonlinear analysis of square concrete-filled double-skin steel tubular columns under axial compression. *Eng. Struct.* **2020**, *216*, 110678. [CrossRef]
17. Rizwan, M.; Liang, Q.Q.; Hadi, M.N.S. Fiber-based computational modeling of rectangular double-skin concrete-filled steel tubular short columns including local buckling. *Eng. Struct.* **2021**, *248*, 113268. [CrossRef]
18. Ding, F.X.; Wang, W.J.; Lu, D.R. Study on the behavior of concrete-filled square double-skin steel tubular stub columns under axial loading. *Structures* **2020**, *23*, 665–676. [CrossRef]
19. Guo, Z.; Chen, Y.; Wang, Y.; Jiang, M.Y. Experimental study on square concrete-filled double skin steel tubular short columns. *Thin-Walled Struct.* **2020**, *156*, 107017. [CrossRef]


**Disclaimer/Publisher's Note:** The statements, opinions and data contained in all publications are solely those of the individual author(s) and contributor(s) and not of MDPI and/or the editor(s). MDPI and/or the editor(s) disclaim responsibility for any injury to people or property resulting from any ideas, methods, instructions or products referred to in the content.